THE JOURNAL OF BIOLOGICAL CHEMISTRY
Vol. 271, No. 36, Issue of September 6, pp. 21956–21968, 1996

Printed in U.S.A.

The 1.5-Å Resolution Crystal Structure of Bacterial Luciferase in Low Salt Conditions*

(Received for publication, April 5, 1996, and in revised form, June 10, 1996)

Andrew J. Fisher‡§, Thomas B. Thompson‡, James B. Thoden‡, Thomas O. Baldwin¶, and Ivan Rayment‡‖

From the ‡Institute for Enzyme Research and Department of Biochemistry, University of Wisconsin, Madison, Wisconsin 53705 and the ¶Department of Biochemistry and Biophysics, Texas A & M University, College Station, Texas 77843

Bacterial luciferase is a flavin monooxygenase that catalyzes the oxidation of a long-chain aldehyde and releases energy in the form of visible light. A new crystal form of luciferase cloned from *Vibrio harveyi* has been grown under low-salt concentrations, which diffract x-rays beyond 1.5-Å resolution. The x-ray structure of bacterial luciferase has been refined to a conventional *R*-factor of 18.2% for all recorded synchrotron data between 30.0 and 1.50-Å resolution. Bacterial luciferase is an α-β heterodimer, and the individual subunits fold into a single domain $(\beta/\alpha)_8$ barrel. The high resolution structure reveals a non-prolyl *cis* peptide bond that forms between Ala^{74} and Ala^{75} in the α subunit near the putative active site. This *cis* peptide bond may have functional significance for creating a cavity at the active site. Bacterial luciferase employs reduced flavin as a substrate rather than a cofactor. The structure presented was determined in the absence of substrates. A comparison of the structural similarities between luciferase and a nonfluorescent flavoprotein, which is expressed in the *lux* operon of one genus of bioluminescent bacteria, suggests that the two proteins originated from a common ancestor. However, the flavin binding sites of the nonfluorescent protein are likely not representative of the flavin binding site on luciferase. The structure presented here will furnish a detailed molecular model for all bacterial luciferases.

Living organisms that radiate light have been captivating people throughout the ages. Bioluminescent organisms such as fireflies, glowworms, mushrooms, fish, or bacteria represent a diverse range of species, which are widely dispersed in nature (1, 2). The enzymes that catalyze the bioluminescence reactions are named luciferases, and in most cases, their substrates are designated luciferins. These enzymes comprise a large evolutionarily diverse group, and the chemistry they catalyze is quite varied. Indeed, the only common factors of these enzymes is the requirement of O_2, which was first established by Robert Boyle (3) more than 3 centuries ago. Today, it is known that all luciferase reactions are oxidative processes that convert a substrate to an electronically excited intermediate. Light emission occurs when the excited-state intermediate reverts back to the ground state resulting in the final product.

Luminous bacteria are the most abundant and widely distributed of all bioluminescent organisms and are found in marine, freshwater, and terrestrial environments. Bacterial luciferase has been studied extensively and is the best understood of all luciferases. The luciferase of luminous bacteria is a flavin monooxygenase. Bacterial luciferase is an uncommon flavoprotein in that it employs reduced flavin as a substrate rather than a tightly bound cofactor. The enzyme catalyzes the reaction of $FMNH_2$, O_2, and a long-chain aliphatic aldehyde to yield FMN, the aliphatic carboxylic acid and blue-green light. All bacterial luciferases studied so far appear to be homologous, and all catalyze the same reaction:

$$FMNH_2 + O_2 + RCHO \rightarrow FMN + RCOOH + H_2O + h\nu(\lambda_{max} = 490\ nm)$$

REACTION 1

The reaction proceeds through a series of intermediates leading to the formation of a C4a hydroxyflavin (for review see Ref. 4). Light emission apparently occurs from this hydroxyflavin, which dehydrates to yield FMN.

Bacterial luciferase is a heterodimeric enzyme of 77 kDa, composed of α and β subunits with molecular masses of 40 and 37 kDa, and in the case of *Vibrio harveyi*, 355 and 324 residues, respectively. The two polypeptides, encoded on adjacent genes, *luxA* and *luxB* in the *lux* operon, display sequence homology and appear to have arisen by gene duplication (4). There is a single active center in the luciferase heterodimer that resides on the α subunit (5) and binds one reduced flavin molecule (6, 7). The role of the β subunit is not clear at this time but is essential for a high quantum yield reaction (8). Amino acid sequence alignment between the two subunits reveals that they share 32% sequence identity. The α subunit contains 29 additional amino acid residues inserted between residues 258 and 259 of the β subunit (9, 10). This region of the α subunit is known to be sensitive to proteolytic digestion in the absence of substrates (11, 12). A single proteolytic cleavage in the region of residues 274–291 in the α subunit inactivates the enzyme (11, 13). The protease labile region of the α subunit appears to move during the catalytic cycle and becomes protected from protease treatment. Binding of $FMNH_2$ to the α subunit reduces vulnerability to proteolytic inactivation (11, 14, 15). The β subunit is insensitive to proteases, and the quaternary structure of the α-β complex is not altered by proteolytic cleavage (13).

Last year, we reported the crystal structure of bacterial

* This research was supported in part by National Institutes of Health Grant AR35186 (to I. R.) and Fellowship AR08304 (to A. J. F.), the Robert A. Welch Foundation Grant A-865 (to T. O. B.), and the Office of Naval Research Grants N00014-93-1-0991, N00014-96-1-87, and N00014-93-J-1345 (to T. O. B.). The costs of publication of this article were defrayed in part by the payment of page charges. This article must therefore be hereby marked "*advertisement*" in accordance with 18 U.S.C. Section 1734 solely to indicate this fact.

The atomic coordinates and structure factors (file accession 1LUC, tracking number T-8732) have been deposited in the Protein Data Bank, Brookhaven National Laboratory, Upton, NY.

§ Present address: Dept. of Chemistry, University of California, Davis, CA 95616.

‖ To whom correspondence should be addressed: Institute for Enzyme Research, 1710 University Ave., Madison, WI 53705. Tel.: 608-262-0529; Fax: 608-265-2904; E-mail: ivan@enzyme.wisc.edu.

TABLE I
Luciferase data collection and refinement statistics

Data collection	
Number of measured reflections	297,839
Number of unique reflections	105,158
Percentage data (30.0–1.50 Å)	99.0
R_{merge} (%)[a]	4.1
Refinement	
Program	TNT
Resolution	30.0–1.50 Å
Number of reflections ($\|F\| > 0$)	105,158
R-Factor (%)[b]	18.2
Root mean square deviations from ideal geometry	
Bond distances	0.015 Å
Bond angles	2.40°
Planar groups	0.007 Å
Non-hydrogen protein atoms (average B)	5,094 (21.00 Å^2)
Solvent molecules	
H_2O (average B)	639 (31.48 Å^2)
Mg^{2+} (average B)	3 (29.00 Å^2)
Ethyleneglycol (average B)	5 (31.40 Å^2)

[a] $R_{merge} = [\sum_h \sum_i |I_h - I_{hi}| / \sum_h \sum_i I_{hi}] \times 100$, where I_h is the mean of the I_{hi} observations of reflection h.
[b] R-Factor = $\sum \| |F_o| - |F_c| \| / \sum |F_o| \times 100$.

luciferase from *V. harveyi* at 2.4-Å resolution (16). That structure was determined by multiple isomorphous replacement from crystals grown in 1.4 M ammonium sulfate, 0.2 M phosphate. Each subunit folds into a single domain $(\beta/\alpha)_8$ barrel motif. Dimerization is mediated through a parallel four-helix bundle centered on a pseudo 2-fold axis that relates the structurally similar subunits. Recently, Conti and co-workers (17) ascertained the crystal structure of firefly luciferase. Firefly luciferase is a 62-kDa monomer that folds into a structure different from bacterial luciferase. This was anticipated since the protein sequence and the chemistry catalyzed by these two luciferases are considerably different.

We report here a new crystal form of bacterial luciferase grown in low-salt conditions that diffract x-rays to significantly higher resolution than the previous crystals grown in high-salt concentrations. The structure was determined at 1.50-Å resolution from a single crystal of bacterial luciferase grown in methyl ether polyethylene glycol, which was frozen at −160 °C. This higher resolution structure has revealed many new features of luciferase including the solvent structure and the observation of a non-prolyl *cis* peptide bond between residues Ala^{74} and Ala^{75} of the α subunit, which may have functional significance. The higher resolution structure categorically defined the geometry of all the residues of the 77-kDa bioluminescent enzyme, with the exception of the protease-sensitive loop, and provides a molecular framework for all bacterial luciferases.

EXPERIMENTAL PROCEDURES

Crystallization and Data Collection—Luciferase, cloned from *V. harveyi*, was expressed in *Escherichia coli* and purified as described earlier (18). A new crystal form of bacterial luciferase was grown under conditions different than previously reported (16, 19). Crystals were grown by micro batch method at 4 °C in 17% methyl ether polyethylene glycol (ME-PEG)[1] (M_r 5000), 250 mM $MgCl_2$, buffered at pH 6.5 with 100 mM MES. The final protein concentration was 7.5 mg/ml. Crystallization was induced by introduction of micro- or macroseeds obtained from preliminary hanging drop experiments. Crystals utilized for seeding were prepared by soaking in 14% ME-PEG for 5 min to dissolve any additional nucleation points. The new crystal form of bacterial luciferase grown in methyl ether polyethylene glycol grew to the size of 0.7 × 0.3 × 0.1 mm in 7 days and diffracts x-rays to better than 1.5-Å resolution at a synchrotron radiation source. A crystal large enough for data collection was transferred directly into a cryoprotectant consisting of 20% ethylene glycol, 22% ME-PEG, 300 mM $MgCl_2$, 50 mM MES, pH 6.5.

After transferring to the cryoprotectant, the crystal was immediately mounted in a loop (20) constructed of 20-μm thick surgical suture and was frozen in the stream of nitrogen (−160 °C) directly on the rotation camera at the Stanford synchrotron radiation laboratory, beam line 7-1 (λ = 1.08 Å). Strong diffraction maxima were observed beyond Bragg spacings of 1.5 Å. Data were collected by oscillation photography. Two scans of a single frozen crystal were employed for data acquisition strategy. The first scan consisted of 1° oscillations for long doses to increase the intensity of the high resolution reflections but resulted in overloading the low resolution data. The exposure time depended on beam energy and varied during the ring fill to equalize the number of photons per exposure. Diffraction data were collected on a MAR image plate system with a crystal to detector distance of 160 mm. After the high resolution data were collected, the crystal to detector distance was increased to 210 mm, and 2.5° oscillation photographs were taken for lower photon counts to record the low resolution data. Diffraction intensities were measured and scaled together with the programs DENZO and SCALEPACK (21, 22). Partial reflections recorded on adjacent images were added together to approximate full reflections.

The crystals belong to the monoclinic space group C2 with unit cell parameters: a = 150.5 Å, b = 59.0 Å, c = 76.5 Å, β = 93.86°. There is one α-β heterodimer in each asymmetric unit (V_m = 2.20 Å^3/Da, solvent content ≈44%). A 99% complete data set to 1.5-Å resolution was collected on a MAR image plate system from a single crystal that was frozen to −160 °C. The overall R_{merge} is 4.1% for all data to 1.5-Å resolution. Table I gives the data collection statistics.

Structure Determination and Refinement—The structure of luciferase grown in ME-PEG was solved by the molecular replacement method (23). The 2.4-Å resolution ammonium sulfate structure was used as a search model in the molecular replacement program AMORE (24). Data between 10.0- and 4.0-Å resolution were used in the rotation search that resulted in a peak of 14.6 σ, the highest false peak was 7.3 σ. The rotated model was applied in a translation search resulting in a single large peak of 47.6 σ and an *R*-factor of 37.9%. The luciferase structure was then refined against all recorded data to 2.0-Å resolution by the conjugate direction algorithm implemented in TNT (25), lowering the *R*-factor to 30.3%. An initial electron density map was computed at 2.0-Å resolution employing SIGMAA coefficients to suppress model bias (26). The resulting map was of excellent quality, and manual adjustments were made with the program **O** (27). The ensuing model was then subjected to another round of TNT refinement, which lowered the *R*-factor to 24.1% for all data to 2.0-Å resolution. Subsequent refinement against all recorded data to 1.50-Å resolution resulted in an *R*-factor of 26.0%, which was reduced to 21.1% with minor manual adjustments of the model and adding 302 water molecules with the programs PEKPIK in TNT (25) and WATPEAK in the CCP4 program suite (28). The final model of the α subunit consists of residues 1–261 and 291–355. The 29 residues (262–290) for which there is no electron density corresponds to the protease-sensitive loop that is also disordered in the ammonium sulfate structure. SDS gel analysis of luciferase

[1] The abbreviations used are: ME-PEG, methyl ether polyethylene glycol; MES, 2-(*N*-morpholino)ethanesulfonic acid; TIM, triose-phosphate isomerase; NFP, nonfluorescent flavoprotein.

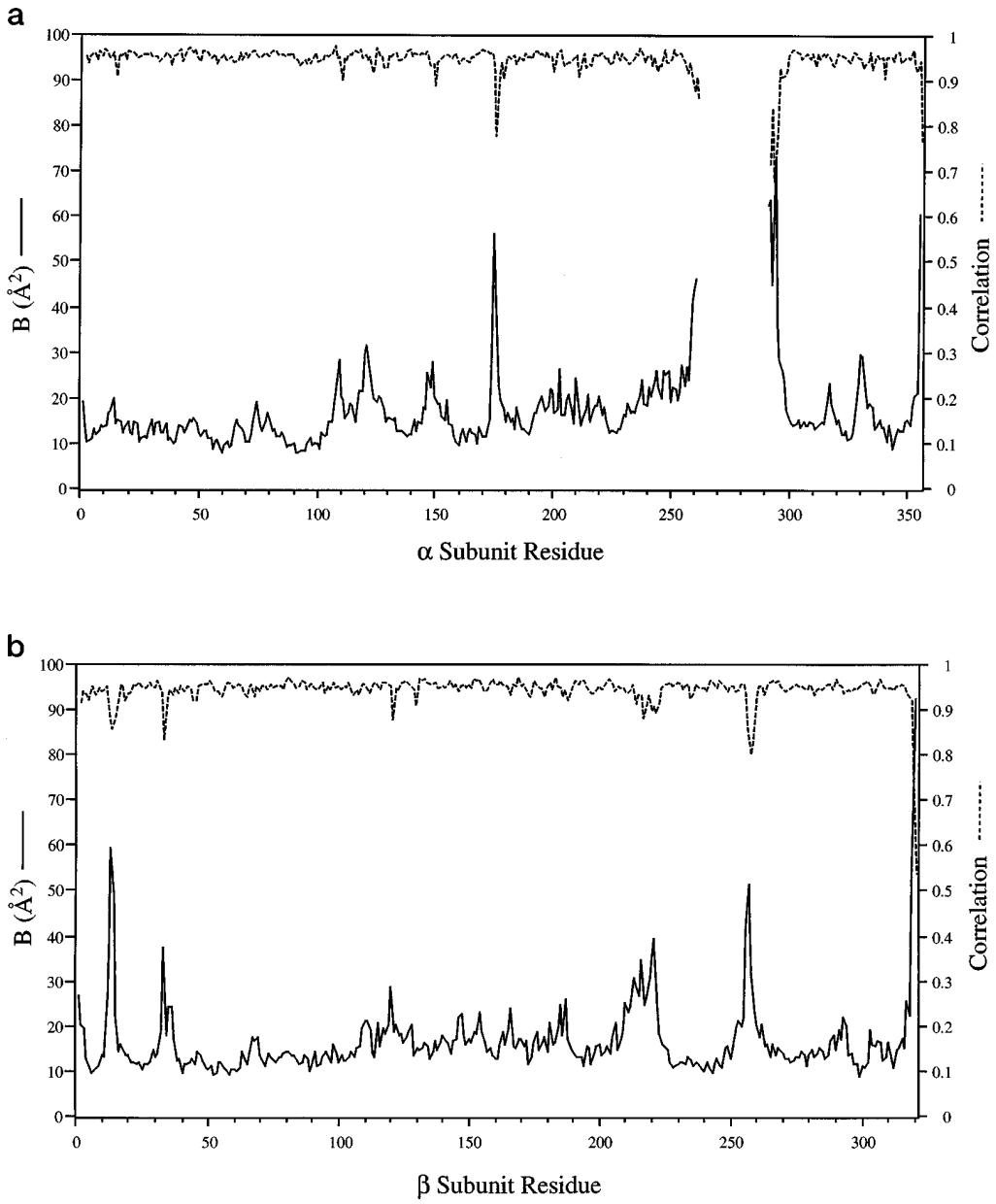

FIG. 1. **Temperature factors.** Plot of main-chain temperature factors (*solid lines*) and correlation (*dashed lines*) for the α subunit (*a*) and β subunit (*b*). The correlation coefficient is a measure of how well the atoms fit the electron density as calculated by the molecular graphics program **O** (27). The mean main-chain temperature factor and correlation coefficient for the α subunit are 16.9 Å^2 and 0.948, respectively, and for the β subunit 16.6 Å^2 and 0.945, respectively.

crystals indicates that both subunits are intact (data not shown). All but the last four amino acids of the β subunit were traced in the electron density map. The final model has an *R*-factor of 18.2% for all recorded data ($|F| > 0$) to 1.50-Å resolution where the root mean square (r.m.s.) deviation from ideal bond lengths, angles, and planes are 0.015 Å, 2.40°, and 0.007 Å, respectively. Table I presents the final refinement statistics including number of atoms and average *B*-values.

A plot of the average main-chain temperature factors and correlation coefficient are shown in Fig. 1, *a* and *b*. The correlation coefficient is a measure of how well the atoms fit the electron density as calculated in the molecular graphics program **O** (27). The mean main-chain temperature factor and correlation coefficient for the α subunit are 16.9 Å^2 and 0.948, respectively, and for the β subunit 16.6 Å^2 and 0.945, respectively.

RESULTS AND DISCUSSION

Structure Description—A Ramachandran plot (29) of the main-chain conformation angles indicates that 99% of the non-glycine residues lie in the allowed regions as defined by the program PROCHECK (30). The average coordinate error in the final model, as estimated from a Luzzati plot (31), is between 0.125 and 0.15 Å. Figs. 7*a* and 9 show a region of representative electron density at 1.50-Å resolution computed with the coefficients of $2|F_o| - |F_c|$ and phases calculated from the final model.

The α-β heterodimer has a parallelepiped shape with dimensions roughly 75 × 45 × 40 Å (Fig. 2). As expected from the sequence similarity, the α and β subunits display similar tertiary structures. Both subunits contain a single $(\beta/\alpha)_8$ barrel that was first observed in the crystal structure of triose-phosphate isomerase (TIM) (32). The α and β subunits have identical topologies (Fig. 3), with the most outstanding loop of the $(\beta/\alpha)_8$ motif existing between β7 and α7.

Hydrophobic residues pack in the β-barrel inner core of both subunits. However, NH_2-terminal residues of the β-strands are hydrophilic and exposed to solvent. Part of the β-barrel's C-terminal end is hydrophobic and shielded from solvent by two α-helices. The α-helices (α7a and α7b) emerge from the β7-α7

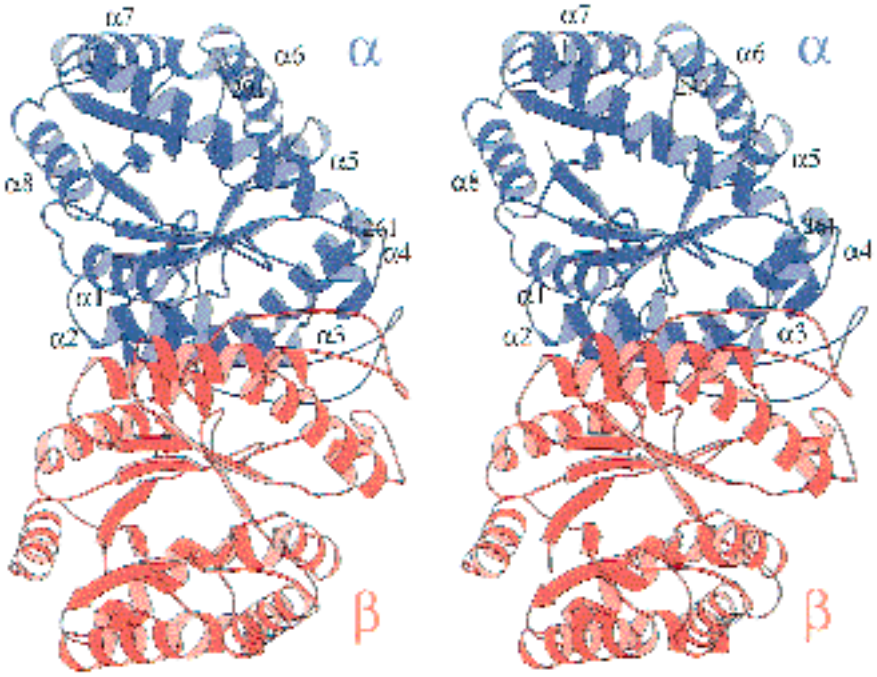

FIG. 2. **Luciferase structure.** Stereo ribbon representation of bacterial luciferase generated with the program MOLSCRIPT (72). The view is perpendicular to the pseudo 2-fold axis that lies horizontal in the plane of the page. The pseudo 2-fold axis relates the α subunit shown in *blue* to the β subunit in *red*. The eight core helices are labeled in the α subunit.

loop. This feature is observed in both α and β subunits. In the β subunit, helix α7a extends along the top of the barrel, followed by a tight turn then helix α7b, which runs antiparallel to helix α7a. In the α subunit, helix α7a stretches toward the subunit interface. The loop that connects helices α7a to α7b is disordered in the electron density map. Residues 262–290 of the α subunit are not seen in the electron density map. The disordered loop in the α subunit corresponds to the 29-residue insert when compared with the β subunit (residues 258–286) and is the loop that is readily cleaved by proteases in the absence of substrates (11, 12, 14). In the α subunit, helix α7b is short, consisting of 5 residues, although its true length may be obscured by the flexibility in the preceding loop. After helix α7b, both subunits contain a 3-residue β-strand (β7a) that runs parallel to and augments β7, which extends past the other β-strands of the β-barrel.

The only other deviations from the $(\beta/\alpha)_8$ topology is a small helix (α4a) that is positioned at the C-terminal end of the β-barrel of each subunit near the subunit interface. There is also a hairpin loop structure in both subunits that runs along the periphery of the subunit interface and embraces the parallel four-helix bundle at the dimer interface. This hairpin loop contains internal main-chain hydrogen bonds, but the main-chain torsion angles are inconsistent with β structure required to designate the loop an antiparallel β-hairpin. Pro^{154}, conserved in both subunits, disrupts the possible β-strand (Fig. 4, *a* and *b*). Furthermore, Pro^{146} disrupts the other strand in the β subunit opposite Pro^{154} (Fig. 4*b*). The reverse turn at the apex of the hairpin loop structure closely resembles a β type III turn, but the carbonyl oxygen of residue *i* does not hydrogen bond with the main-chain amide nitrogen of residue *i* + *3*. This structure is observed in the hairpin loops of both subunits. Also in both subunits, the residue at position *i* of the turn is Asn^{148}, which favors β reverse turns because the Oδ-1 atom hydrogen bonds to the main-chain amide nitrogen of residue *i* + *2* as is observed in both luciferase subunits. The hairpin loops in both subunits terminate with Pro^{160} whose peptide bond adopts the *cis* configuration in both subunits. Pro^{160} is conserved among all luciferase α and β subunits suggesting the importance of a *cis* peptide bond conformation at this position.

Dimerization is mediated through a parallel four-helix bun-

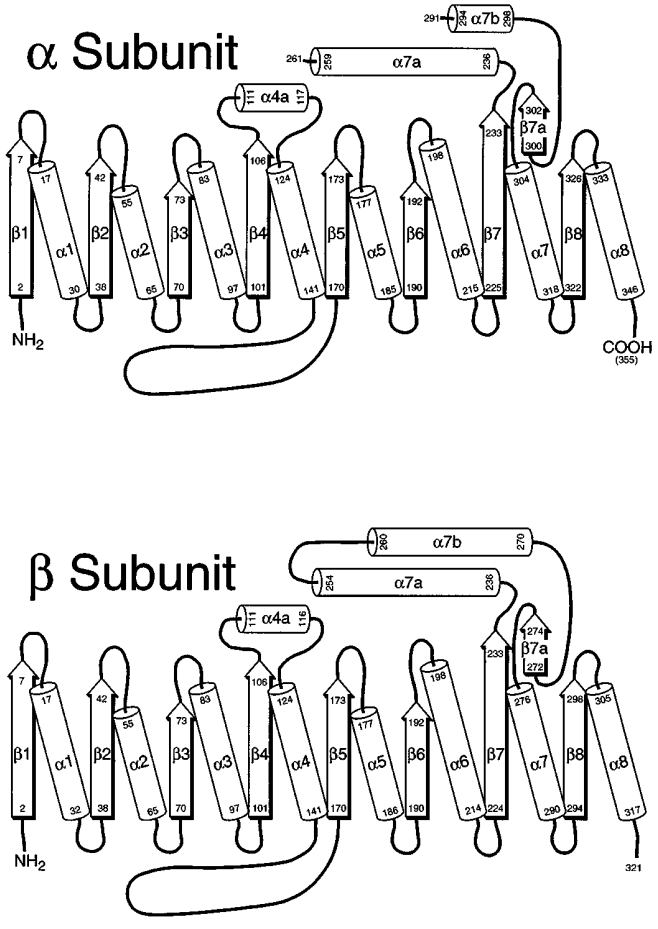

FIG. 3. **Topology diagram.** Cartoon showing the secondary structural elements of the two luciferase subunits (adapted from Ref. 16). β-Strands and α-helices are represented by *arrows* and *cylinders*, respectively. The $(\beta/\alpha)_8$ core is drawn flat along the middle with the loop insertions drawn above and below the core. β8 wraps around and hydrogen bonds to β1 to form the *closed barrel*. The *numbers* refer to the beginning and end of each secondary structural element.

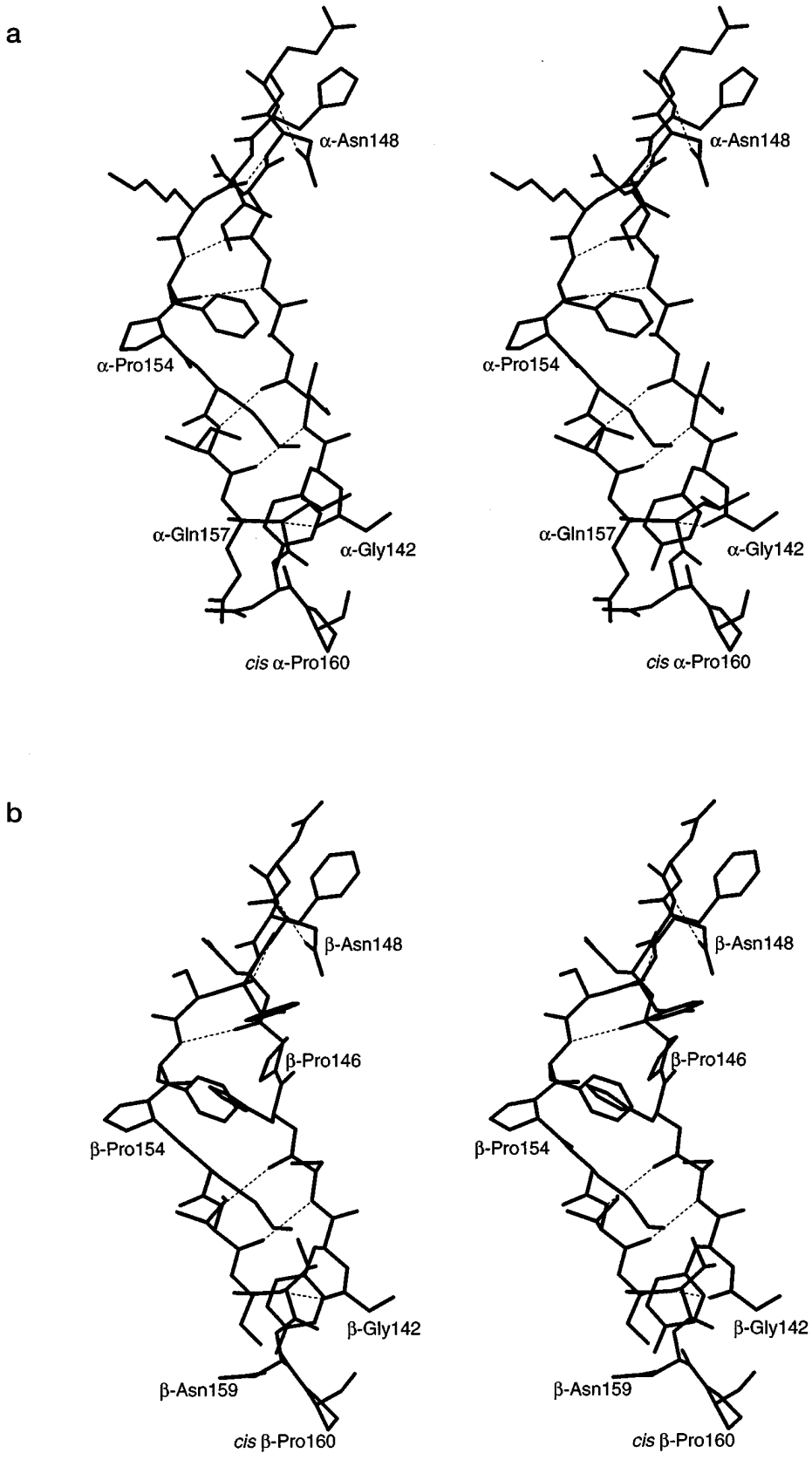

FIG. 4. **Hairpin loop structures of bacterial luciferase.** These loops are observed at opposite ends of the subunit interface and embrace the parallel four-helix bundle. *a*, α subunit hairpin loop displayed as *solid lines* with main-chain hydrogen bonds shown as *dashed lines*. *b*, β subunit hairpin loop viewed in a similar orientation as in *a* for easier comparison. Proline 146 of the β subunit disrupts a main-chain hydrogen bond that is observed in the α subunit. The parallel four-helix bundle at the subunit interface would lie behind the hairpin loops as viewed.

dle, which is centered on a pseudo 2-fold axis that relates the α and β subunits (Fig. 2). Each subunit contributes helices α2 and α3 to form the four-helix bundle. Helix α2 lies very close to the pseudo 2-fold axis resulting in an unusually close packing of the α2 helices from each subunit. At one point, the main chain atoms from one helix reside within 3.2 Å from the main chain atoms in the pseudo 2-fold-related helix in the other subunit. In this region, glycines and alanines shape the surface of the helix allowing for the close contact. In particular, Gly^{64} is totally conserved in all luciferase α and β subunits permitting this intimate contact.

There are a considerable number of intersubunit interactions

TABLE II
Bacterial luciferase intersubunit hydrogen bonds

α Subunit		β Subunit		Bond distance
Residue	Atom	Residue	Atom	
				Å
Gln^{17}	Oε-1	His^{61}	N	2.92
Thr^{18}	Oγ-1	Gln^{95}	Oε-1	3.12
His^{45}	Nδ-1	Glu^{88}	Oε-1	2.57
His^{45}	Nδ-1	Glu^{88}	Oε-2	3.08
Asn^{54}	Nδ-2	Glu^{88}	Oε-2	2.97
Asn^{54}	Oδ-1	Glu^{89}	N	3.48
Thr^{80}	O	Arg^{85}	Nη-2	3.02
Thr^{80}	Oγ-1	Arg^{85}	Nη-2	3.14
Arg^{85}	Nη-2	Thr^{80}	O	2.92
Arg^{85}	Nη-2	Thr^{80}	Oγ-1	3.00
Glu^{88}	Oε-1	His^{45}	Nδ-1	2.67
Glu^{88}	Oε-2	His^{45}	Nδ-1	3.10
Asp^{89}	Oδ-1	Thr^{57}	Oγ-1	2.59
Gln^{95}	Nε-2	Asp^{18}	Oδ-2	2.82
Arg^{115}	Nη-1	Ser^{152}	O	2.98
Val^{116}	O	His^{82}	Nε-2	2.71
Gln^{157}	Nε-2	Asn^{48}	Oδ-1	3.05
Asn^{159}	Nδ-2	Ser^{47}	O	2.81
Asn^{159}	Nδ-2	Gly^{50}	O	3.22
Ser^{161}	N	Ser^{17}	Oγ	2.91
Ser^{161}	Oγ	Ser^{17}	Oγ	3.35
Ser^{161}	Oγ	Asp^{18}	Oδ-1	3.05

arising from the dimer interface. Most of these contacts occur in the parallel four-helix bundle. The majority of intersubunit contacts established in the four-helix bundle are van der Waals interactions. 2150 $Å^2$ of accessible surface area is buried upon dimer formation based on a search probe radius of 1.4 Å (33). This value falls in the expected range given the size of the luciferase subunits (34). Twenty-two intersubunit hydrogen bonds help tether the two subunits together (Table II). An interesting hydrogen bond occurs between residues His^{45} and Glu^{88}. These two residues are conserved among the α and β subunits creating similar intersubunit hydrogen bonds related by pseudo 2-fold symmetry ($His^{\alpha 45}$ H-bonds to $Glu^{\beta 88}$ and $His^{\beta 45}$ to $Glu^{\alpha 88}$). Both of these residues are conserved among all bacterial luciferase α and β subunits, and mutating His^{45} in the α subunit of *V. harveyi* luciferase results in a substantial decrease of bioluminescence activity (35). Another intriguing interaction occurs between $Arg^{\alpha 85}$ and $Thr^{\beta 80}$. The side chain of $Arg^{\alpha 85}$ extends across the subunit interface, and the guanido group is in hydrogen bonding distance with both the Oγ-1 and the carbonyl oxygen of $Thr^{\beta 80}$. These two residues are also totally conserved among all luciferase subunits resulting in a similar interaction between the pseudo 2-fold-related residues. Arg^{85} also points toward Glu^{43}, which again is conserved among all luciferase subunits, but is 3.7 and 4.4 Å away from the carboxylate group in the α and β subunits, respectively. These residues line a large surface accessible cavity that is formed at the dimer interface (Fig. 5). Many ordered water molecules dwell in this pocket. There are also 45 water-mediated intersubunit hydrogen bonds where an atom from each subunit is within hydrogen bonding distance to the same water molecule.

In addition to the polar contacts discussed above, there are also a substantial number of hydrophobic interactions involved in dimer formation. Hydrophobic intersubunit contacts are found between the hairpin loop structure in one subunit and the C-terminal end of helix α4a plus a region of the β2-α2 loop of the other subunit. The C-terminal region of helix α3 establishes hydrophobic contacts with the N-terminal region of helix α1 in the other subunit. Most of the hydrophobic interactions are conserved among the subunits resulting in pseudo symmetric interactions.

A great deal of sequence conservation exists between the two luciferase subunits. Many of the conserved residues are also preserved in the luciferases from other bioluminescent bacteria. Thirty residues are totally conserved among all bacterial luciferase α and β subunits whose sequences are known presently (8, 36). A majority of the conserved residues dwell near the luciferase α-β dimer interface (Fig. 6). This demonstrates that the pseudo 2-fold axis, which relates the α and β subunits, is also evident at the level of the primary structure. Furthermore, conservation of the 2-fold symmetry at the interface suggests its significance for dimerization and enzyme function. This is confirmed by the mutational and structural studies described above. Similar intersubunit interactions are also observed between these residues in the crystal structure of the LuxB homodimer.[2]

Non-prolyl Cis Peptide Bond—In the α subunit, β-strand 3 terminates with a bulge that protrudes into the core of the β-barrel. This bulge contains a *cis* peptide bond between residues Ala^{74} and Ala^{75}. Fig. 7*a* illustrates the conformation of β3 with the bulge and the *cis* peptide displayed with the electron density map. The 1.5-Å resolution electron density map unequivocally demonstrates the *cis* conformation of the peptide bond between residues Ala^{74} and Ala^{75} in the α subunit (Fig. 7*a*). In the 2.4-Å resolution ammonium sulfate structure, the bulge did not fit the density extremely well, but the map was not high enough resolution to confidently build a *cis* peptide bond. A similar bulge terminates β3 in the β subunit, but the density clearly indicates a *trans* peptide bond between Leu^{74} and Asn^{75}. Fig. 7*b* illustrates the similarity of the bulge and overall shape of β3 between the two subunits.

Non-prolyl *cis* peptide bonds are rare (37, 38) but have been observed in a few other crystal structures, and almost all play significant roles in positioning crucial residues to carry out ligand binding and/or catalysis (39). In luciferase, the *cis* peptide bond occurs in a bulge at the end of β3 positioning it at the C-terminal end of the barrel, where all $(\beta/\alpha)_8$ barrels exhibit their active sites (40). Ala^{74} and Ala^{75} form the bottom floor at the entrance of a small cavity projecting off the larger and deeper pocket in the center of the β-barrel of the α subunit (Fig. 8). The walls of this smaller cavity include $His^{\alpha 44}$ on one side

[2] A. J. Fisher, H. M. Holden, J. F. Sinclair, J. B. Thoden, T. O. Baldwin, and I. Rayment, unpublished results.

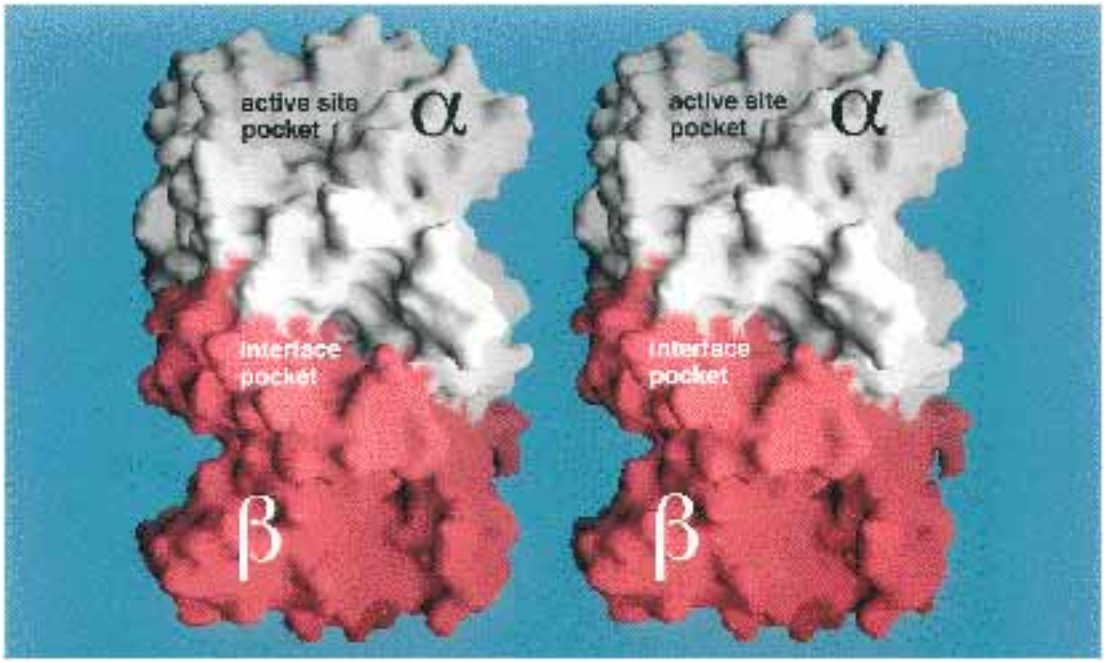

FIG. 5. **Luciferase surface.** Stereo view surface rendering of bacterial luciferase generated with the program GRASP (73). The surface formed from α subunit residues is colored *white* and the β subunit is colored *red*. The *deep pocket* at the subunit interface is clearly visible as well as part of the *active site pocket* in the α subunit.

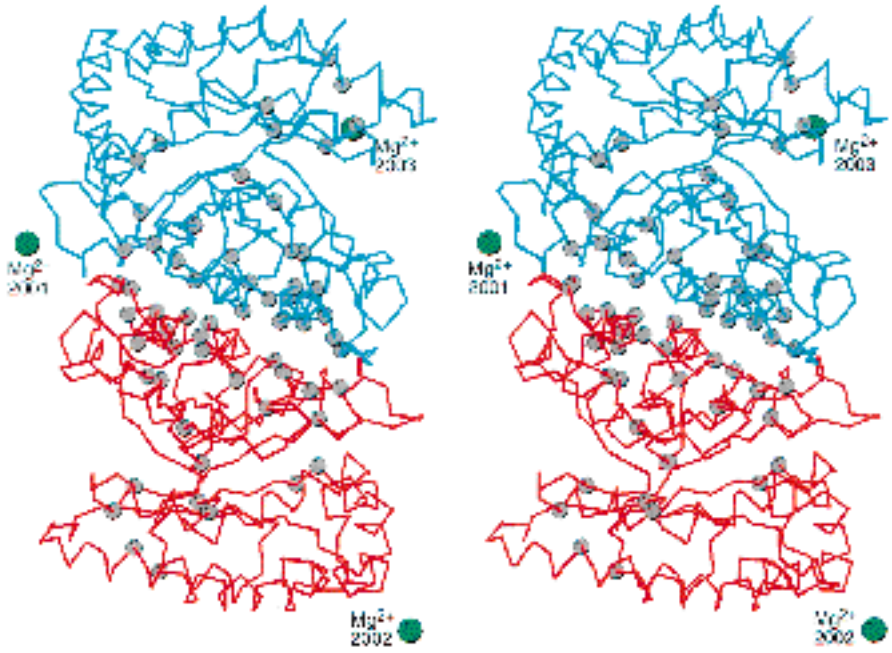

FIG. 6. **Conserved residues.** Stereo α-carbon trace mapping the location of 30 residues that are conserved in all luciferase α and β subunits. The luciferase backbone is drawn in *blue* and *red lines* to designate the α and β subunits, respectively, and α-carbon of each conserved residue is drawn as a *gray ball*. The locations of the three Mg^{2+} ions are also identified by *green balls*. Mg^{2+} ions labeled 2001 and 2002 are involved in crystal contacts while Mg^{2+} 2003 is likely the result of nonspecific binding.

and $Cys^{\alpha 106}$ on the other. Mutation of $His^{\alpha 44}$ to Ala or Asp results in inactivation of the enzyme (35). Cys^{106} of the α subunit is a highly reactive thiol whose chemical modification resulted in inactivation of the enzyme (41, 42). However, site-directed mutagenesis experiments have clearly demonstrated that the reactive thiol is not involved in the bioluminescence reaction (18). Binding of either FMN or $FMNH_2$ in the presence of O_2 to luciferase protects the reactive thiol from modification (41), and modification of the $Cys^{\alpha 106}$ thiol substantially decreases the affinity of the protein for $FMNH_2$ (43). However, modification of the reactive thiol has little effect on the binding of FMN (44). These observations suggest that there is not a direct interaction of the flavin with the thiol that affects protection but rather a conformational change resulting from flavin binding.

These data demonstrate the importance of the small cavity projecting off the central large pocket and could justify the reason for the *cis* peptide bond, because a *trans* conformation would decrease the size of the opening. Residue 75 of the α subunit is either an alanine or glycine residue in all luciferases. Proline, which is more energetically favorable in *cis* peptides, would introduce a larger side chain and reduce the size of the opening. Additionally, the main-chain dihedral angles for $Ala^{\alpha 75}$ ($\phi = -153.1$, $\psi = 164.5$) are unfavorable for proline residues, which prefer to reside around $\phi \approx -60$.

As seen in Fig. 8, two residues from the β subunit also play a role in the small cavity. Glu^{88} from the β subunit hydrogen bonds to $His^{\alpha 45}$, which forms part of the cavity sidewall. This intersubunit interaction, as pointed out above, is conserved in all luciferase subunits. In addition, the guanido group of $Arg^{\beta 85}$

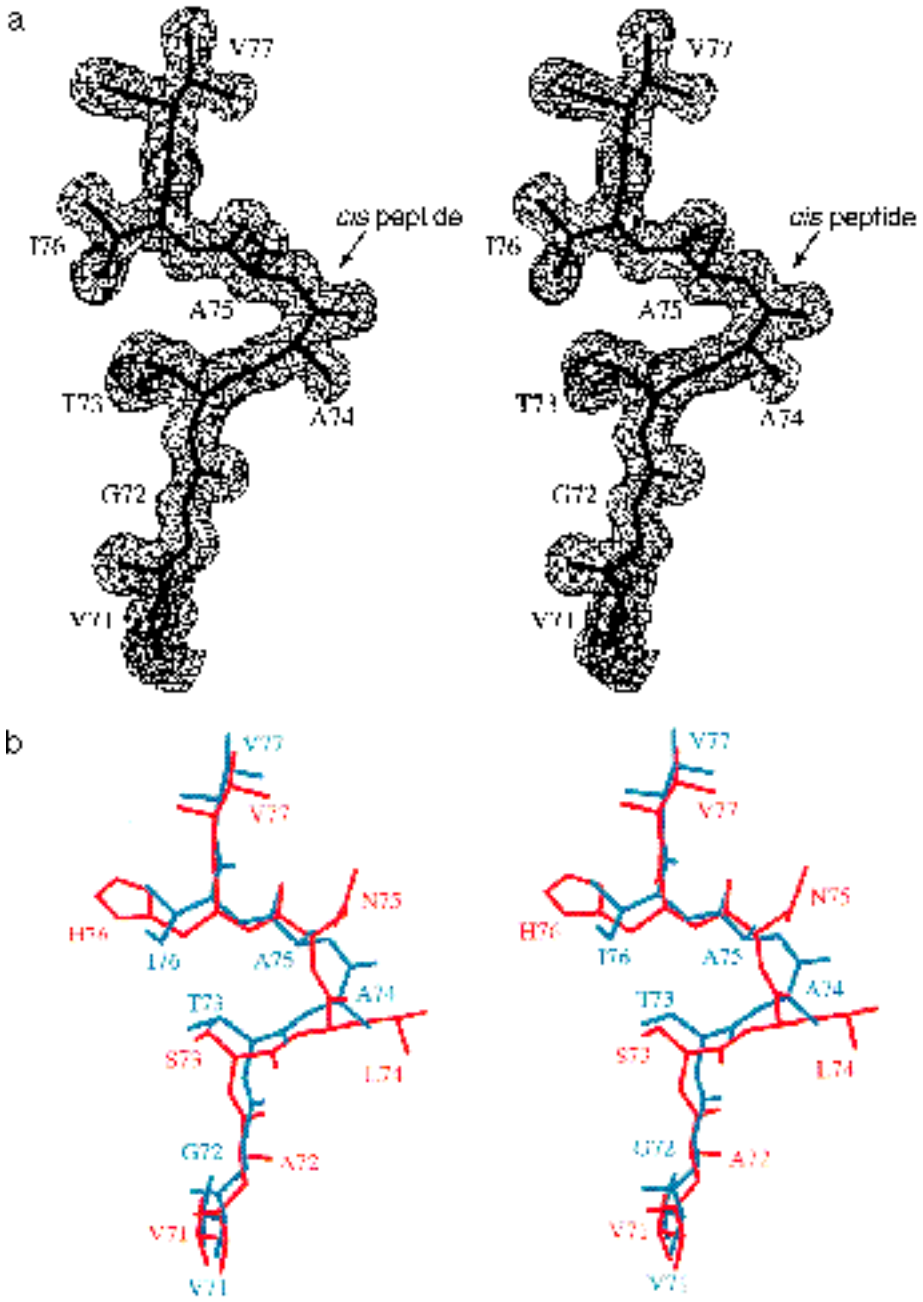

FIG. 7. **Non-prolyl *cis* peptide bond.** *a*, atomic model (*thick lines*) exhibiting the *cis* conformation of the peptide bond between Ala^{74} and Ala^{75} of the α subunit. The final $2F_o - F_c$ electron density map contoured at 1σ is shown as *thin lines* in the stereo view. The bulge at the end β3 (Thr^{73}) projects into the β-barrel core. *b*, a stereo view showing the comparison of strand β3 and the *cis* peptide bulge. The atomic model for the α and β subunits is shown in *blue* and *red lines*, respectively. Both subunits exhibit a similar structure, yet the α subunit requires a *cis* peptide bond which may have functional significance. This figure and Fig. 9 were drawn with the program MolView (74).

forms the back of the cavity. Arg^{85} is also mentioned above for its conserved interactions between subunits. These two residues might suggest a possible role for the β subunit during the bioluminescent reaction if this cavity, which extends off the larger pocket at the C-terminal end of the barrel, is part of the active site. The cavity in the β-subunit is more confined because of a *trans* peptide bond between positions 74 and 75, and larger residues line the cavity's entrance; Asn replaces Ala at position 75 and Tyr substitutes for Leu at position 42.

Magnesium Binding and Crystal Packing—Crystallization of luciferase in methyl ether polyethylene glycol requires the presence of magnesium. Omission of magnesium results in no crystal growth. Removal of magnesium from crystals, by addition of EDTA, results in cracking. During the first manual rebuilding, it became evident why magnesium was required for crystallization. A total of three magnesium ions were observed in the crystal structure (Fig. 6). Two magnesium ions are involved in crystal contacts between symmetry related dimers and the third ion binds to the α subunit but does not have any functional or structural capacities.

One magnesium ion (Mg^{2+} 2002) involved in crystal packing is coordinated by Oϵ-1 of $Glu^{\beta 237}$ and Oδ-1 of $Asp^{\alpha' 346}$ in a symmetry related subunit (Fig. 9) (prime Greek letters represent crystallographic symmetry related subunits). Four ordered water molecules complete the octahedral geometry. The Mg^{2+}-oxygen coordination distances range from 2.03 to 2.33 Å.

Oϵ-1 of $Glu^{\alpha 19}$ coordinates the other magnesium ion involved in crystal packing (Mg^{2+} 2001), and the five remaining Mg^{2+} ligands are ordered water molecules. The carboxylate group of $Glu^{\beta' 130}$ from a symmetry related subunit hydrogen bonds to two of the five Mg^{2+} water ligands. Water molecule 3101 is 2.75 Å away from Oϵ-1 of $Glu^{\beta' 130}$, and the distance between Oϵ-2 of $Glu^{\beta' 130}$ and water 3177 is 2.76 Å.

The third magnesium ion seen in the crystal structure (Mg^{2+} 2003) is not involved in any crystal contacts but binds to the periphery of the α subunit. No protein atoms directly ligate the Mg^{2+}. Six ordered water molecules coordinate the ion with octahedral geometry. This magnesium ion binds near the N-

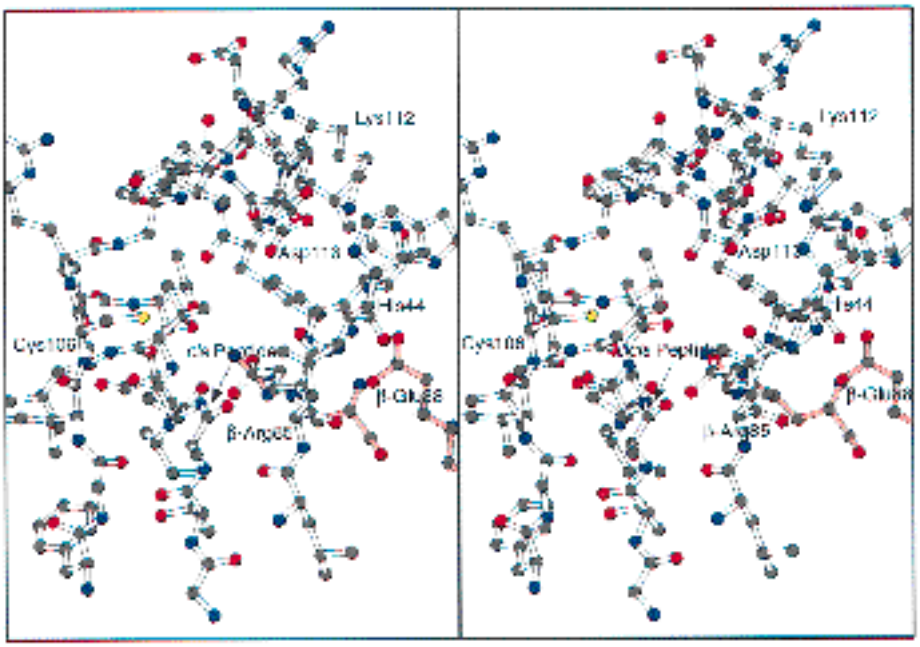

FIG. 8. **Active site cavity.** Stereo ball-and-stick rendering of the small cavity that projects off the main active site pocket at the α subunit's C-terminal portion of the β-barrel. The small cavity is lined by the *cis* peptide bond on the bottom, Cys^{106} whose modification occludes substrate binding, and His^{44}, that when mutated (35) inactivates the enzyme. Also illustrated, with *red bonds*, is Arg^{85} from the β subunit that forms the back wall of the cavity and Glu^{88} from the β subunit that hydrogen bonds to His^{45}.

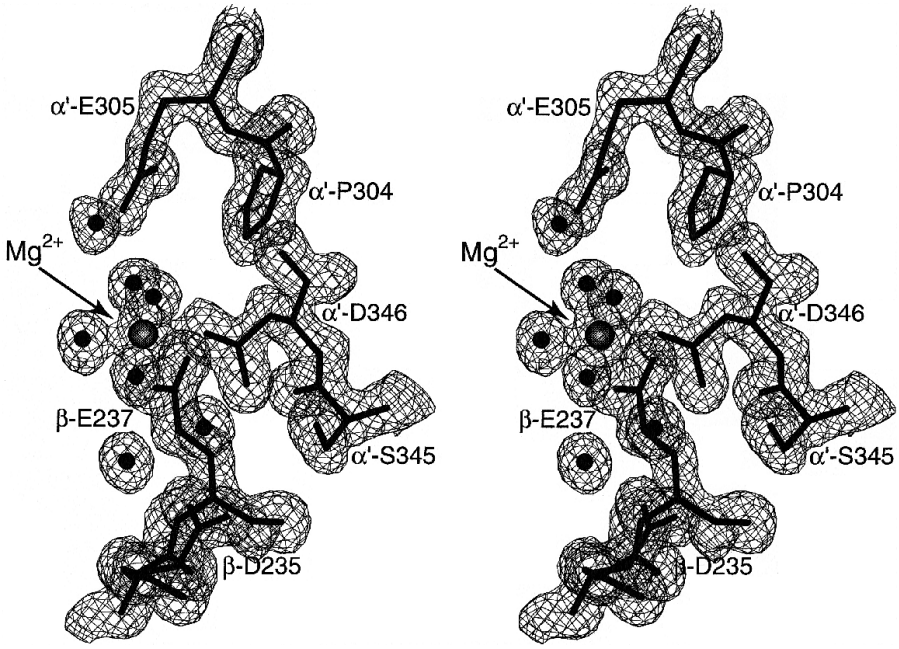

FIG. 9. **Mg^{2+} binding site.** A stereo view illustrating the Mg^{2+} 2002 binding site involved in crystal contacts. The atomic model is displayed as *thick lines*; *prime numbers* represent a crystallographic symmetry related subunit. The Mg^{2+} and the waters that coordinate it are shown as a *large gray* and *small black balls*, respectively. The final electron density map is portrayed in *thin lines*.

terminal opening of the β-barrel and interacts with residues in the loops preceding β strands β7 and β8 of the α subunit (Fig. 6). Six protein atoms hydrogen bond to five of the water ligands. The Oδ-2 atom of $Asp^{\alpha 223}$ and the Oδ-2 of $Asp^{\alpha 321}$ hydrogen bond to the same water ligand (3418), 2.75 and 2.70 Å, respectively. Oδ-1 of $Asp^{\alpha 321}$ hydrogen bonds to water 3335. The main-chain carbonyl oxygen of $Lys^{\alpha 221}$ is 2.91 Å away from water ligand 3352, and the carbonyl oxygen of $Ile^{\alpha 222}$ is 3.18 Å away from water ligand 3380. The amine group of $Lys^{\alpha 2}$ hydrogen bonds to Mg^{2+} ligating waters 3418 and 3486. The binding site of this magnesium ion was unexpected but probably does not have any functional significance since no protein atoms directly ligate the Mg^{2+}. Furthermore, the *B*-factors of the third Mg^{2+} and its coordinated waters are approximately 15 $Å^2$ higher than for the other two Mg^{2+} sites involved in crystal contacts, suggesting this binding might be nonspecific and a result of the high $MgCl_2$ concentration used in crystallization.

In addition to the magnesium ions binding to the luciferase structure, five well ordered ethylene glycol molecules are apparent in the solvent structure. Ethylene glycol was used as a cryo-protectant to preserve the crystal during freezing at −160 °C. All five ethylene glycols bind at the protein surface, three of them at the α-β subunit interface. One of the ethylene glycol molecules binds in a small cavity that is formed between helices α1 and α2 of the α subunit. Another ethylene glycol molecule mediates an intersubunit contact. His^{82} from the α subunit hydrogen bonds to a glycol hydroxyl oxygen, which in turn hydrogen bonds to the carbonyl oxygen of Phe^{226} in the β subunit. In all five cases, one or both ethylene glycol hydroxyl oxygens hydrogen bonds to the protein.

Structural Similarities—There is extensive structural conservation between the α and β subunits confirming their common origin (4). The topology of the α and β subunits is identical, and the secondary structural elements align exactly with the sequence (Fig. 10). The two luciferase subunits superimpose

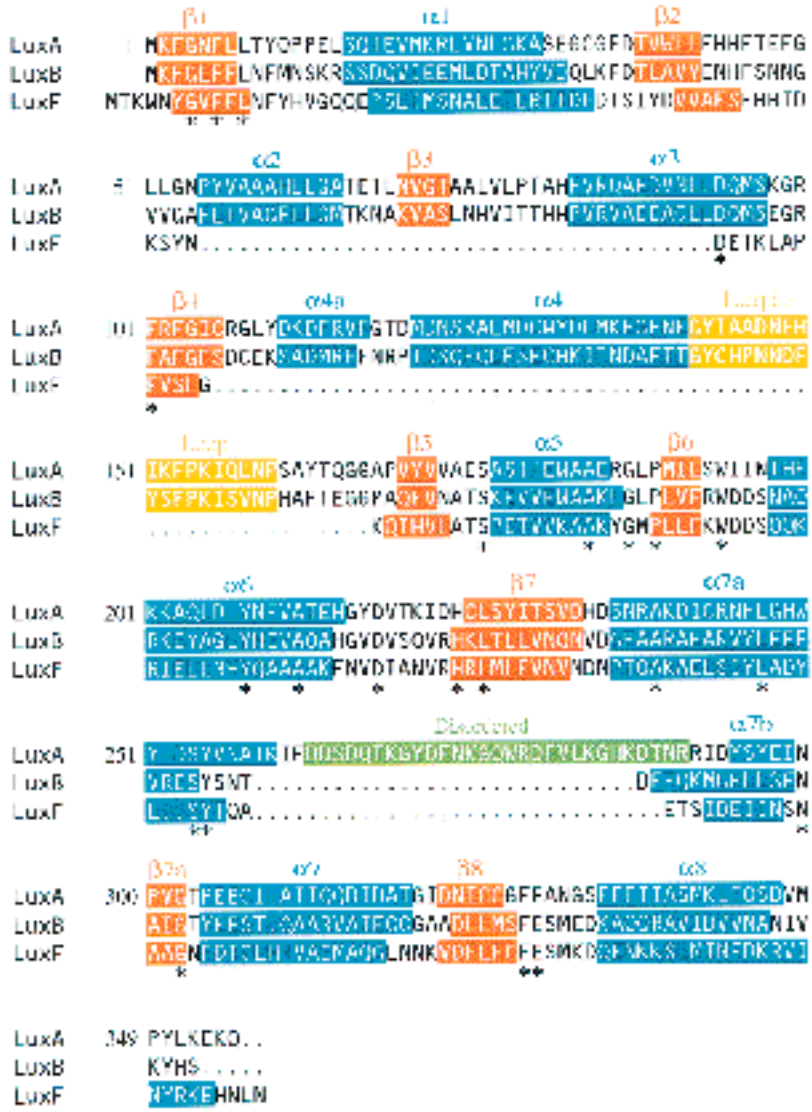

FIG. 10. **Sequence alignment.** Protein sequence alignment of luciferase α and β subunits from *V. harveyi* (*LuxA* and *LuxB*) and nonfluorescent protein from *P. leiognathi* (*LuxF*). Alignment was based on sequence and secondary structural elements from the crystal structures. The luciferase α and β subunits share 31.9% sequence identity, whereas NFP is 22.4 and 33.3% identical to the luciferase α and β subunits, respectively. The secondary structural elements, as observed in the crystal structures, are displayed above the sequence and by *colored boxes*. The *asterisks* label residues that are conserved in all three proteins.

with a root mean square deviation of 1.99 Å for 300 equivalent α-carbons (Fig. 11*a*). The structures of the β-barrels are very similar with only a 0.61-Å r.m.s. deviation in the superposition of the barrel's 39 α-carbons. Most of the differences in the α-β superposition occur in the exterior α-helices, which are slightly displaced relative to their pseudo 2-fold-related subunit. The largest displacement appears in the short helix α4a near the C-terminal end of the β-barrel. Helix α4a in the α subunit shifts approximately 3 Å along the helix axis away from the barrel's center permitting a larger opening to the active site. The regions involved with dimerization, helices α2 and α3 and the hairpin loop structure, are exceptionally similar in structure.

Structural similarities were also observed between the luciferase subunits and the nonfluorescent flavoprotein (NFP) (45, 46) from *Photobacterium leiognathi*. Bioluminescent bacteria belonging to the genus *Photobacterium* contain an additional gene located between *luxB* and *luxE* in the *lux* operon. This gene now known as *luxF*, was originally designated *luxG* (47), and independently as *luxN* (48). The *luxF* gene encodes a 24-kDa nonfluorescent flavoprotein whose function is unknown at present but binds two molecules of an unusual flavin mononucleotide adduct (45, 46, 49). Myristic acid is covalently linked to C-6 of the isoalloxazine ring of the flavin mononucleotide. Interestingly, both myristic acid and FMN are end products of the luciferase bioluminescence reaction. However, the connection between the nonfluorescent flavoprotein and bioluminescence remains unclear. NFP displays sequence similarity to both luciferase subunits and is 22.4 and 33.3% identical in amino acid sequence to the luciferase α and β subunits, respectively (Fig. 10).

The crystal structure of NFP has been recently determined (49) and refined to high resolution (50). The crystal structure revealed that NFP forms a homodimer, and each monomer folds into a novel seven-stranded β-barrel surrounded by seven α-helices. Given the NFP structure and sequence alignment of *luxF* to *luxA* and *luxB*, Moore and James (51) correctly predicted the structure of the luciferase monomer to have a $(\beta/\alpha)_8$ fold. The structure of NFP superimposes surprisingly well with the individual luciferase α and β subunits, 2.48 and 1.55 Å r.m.s. deviation, respectively (Fig. 11*b*). The NFP β-barrel is mostly parallel (strands β3 and β4 form an antiparallel hairpin) and contains a considerable gap between strands β2 and β3. The seven NFP β-strands align well structurally with seven of the eight luciferase strands. In the superposition, strand β3 of luciferase (α and β subunits) resides in the gap between strands β2 and β3 of NFP that would complete an eight-stranded β-barrel (Fig. 11*b*). In the NFP structure, this gap is filled with ordered water molecules that fasten the two ends of the barrel together with a hydrogen bonding network to strands β2 and β3 (50). It is interesting to point out that the

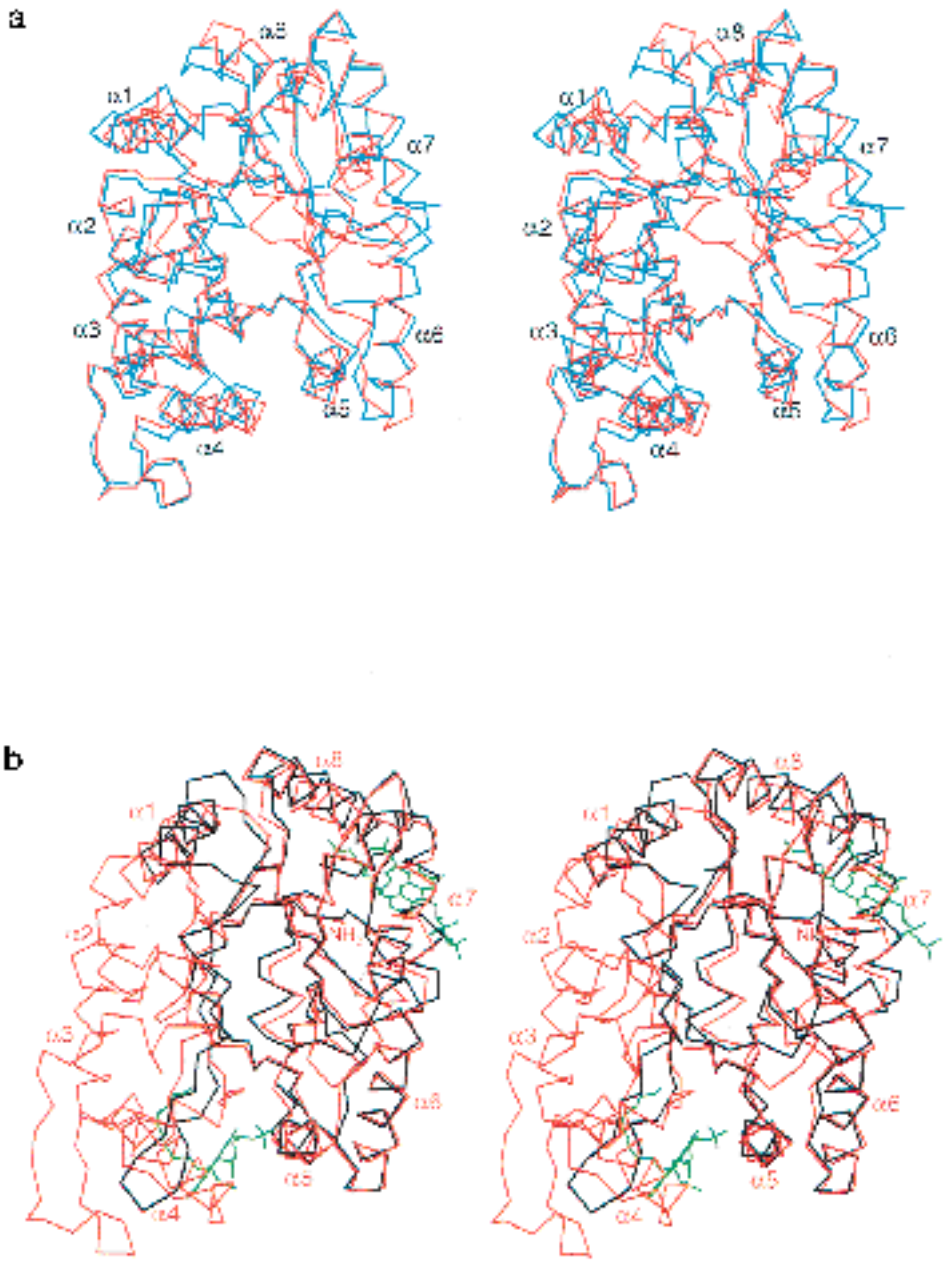

FIG. 11. **Luciferase structural comparison.** *a*, superposition of the luciferase α and β subunits drawn in stereo. The α-carbon trace is drawn in *blue* and *red* to delineate the α and β subunits, respectively. The two subunits superimpose with an r.m.s. deviation of 1.99 Å for 300 equivalent α-carbons. *b*, stereo superposition of LuxF NFP (*black lines*) onto the luciferase β subunit (*red lines*). NFP superimposes onto the β subunit with an r.m.s. deviation of 1.55 Å for 132 equivalent α-carbons. The myristoylated flavin adduct bound to NFP is drawn in *green bonds*.

strand missing in the NFP structure is the same strand that terminates with a non-prolyl *cis* peptide bond in the luciferase α subunit. Strand β3 of NFP structurally aligns with β4 of luciferase in the superposition but runs in the reverse direction.

The seven helices of NFP align with helices α1, α5, α6, α7a, α7b, α7, and α8 of the luciferase α and β subunits (Figs. 10 and 11*b*). NFP does not contain residues or secondary structural elements corresponding to the helices and the hairpin loop involved in the luciferase dimerization. Sequence alignment of NFP to luciferase α and β subunits reveals a gap in the NFP sequence corresponding to helices α2, α3, β-strand β3, and the hairpin loop (Fig. 10). However, homo-dimerization of NFP still occurs along the same relative region of the molecule, but the intersubunit interactions occur between β-strands (49, 50) and not helices as observed in luciferase. Additionally, the β7-α7 loop in the luciferase β subunit, which contains helices α7a and α7b and the short strand β7a that augments β7, is also seen in NFP and superimposes with an r.m.s. deviation of 0.79 Å.

This evidence suggests that *luxF* may have arisen from gene duplication of *luxB* (luciferase β subunit) and subsequently lost its ability to associate with the *luxA* gene product by deletion of the residues involved in dimerization. Yet LuxF still maintained (or developed) its ability to form homodimers. The function of LuxF, which is found in only one genus of bioluminescent bacteria, is unknown, but is not required for bioluminescence (36).

The locations of the two unique flavin adducts that bind to NFP are shown in Fig. 11*b*. Both flavin cofactors bind on the side of the β-barrel between the surface helices. These binding sites probably do not reveal the flavin active site in luciferase, because helices α4 and α8 in luciferase extend over the equivalent flavin binding sites and would occlude FMN binding. Moreover, both sites are distant from the C-terminal end of the

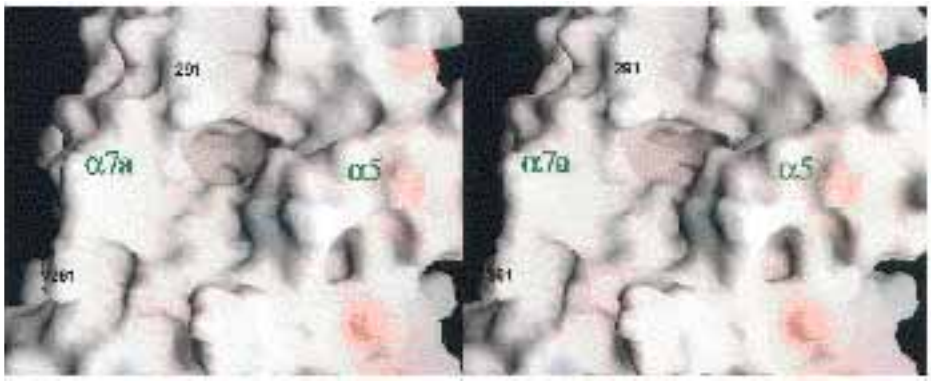

FIG. 12. **Active site pocket surface map.** Stereo view of the molecular surface illustrating the size and depth of the active site pocket in the luciferase α subunit. The molecular surface was drawn with the program GRASP and color-coded by electrostatic potential. The small cavity bordered by the *cis* peptide bond is projecting down out of view in the pocket. Residues that flank the disordered loop and helices α5 and α7a of the α subunit are labeled for orientation.

α subunit's β-barrel, which is the location of the active site in enzymes that exhibit the $(\beta/\alpha)_8$ motif (40). The phosphate moiety of the flavin molecule that binds near the N terminus of helix α5 in NFP is 3.2 Å away from the phosphate binding site seen in the luciferase structure previously determined in ammonium sulfate (16). This region was hypothesized to bind the phosphate moiety of reduced flavin in luciferase (16). By anchoring the phosphate moiety of $FMNH_2$ at this site, the flavin can be modeled extending across the C-terminal portion of the α subunit β-barrel. This positions the isoalloxazine ring next to Trp^{194} and Trp^{250}, which have been implicated to interact with the flavin ring as measured by fluorescence spectroscopy and circular dichroism spectroscopy.[3] A phosphate ion was not observed in the ME-PEG structure because phosphate was not included in the crystallization conditions.

The regions of high temperature factors in the α subunit correspond to loops that have been proposed to bind flavin (16). The peaks in the α subunit temperature factor plot (Fig. 1*a*) around residues 109, 121, and 175 all map to loops in the vicinity of the phosphate binding site that was observed in the structure of luciferase derived from crystals grown in ammonium sulfate. The high thermal parameters in the phosphate-free structure suggest flexibility in these areas, which would become stationary upon binding reduced flavin.

There appears to be no significant differences between the structure of luciferase solved in ME-PEG and the original structure solved in ammonium sulfate. Superposition of 630 equivalent α-carbons results in an r.m.s. deviation of 0.59 Å between the two structures. This value falls in the range observed for other proteins whose structures have been determined from different space groups (52, 53). Furthermore, in addition to the differences described above, more of the α-subunit's α7a-α7b loop is disordered in the ME-PEG structure, which contains 13 fewer ordered residues.

Active Site Pocket—The active sites of all $(\beta/\alpha)_8$ barrel enzymes reside at the C-terminal end of the β-barrel (40). In most cases, residues in the loops that connect the β-strand to the subsequent α-helix fabricate the active site. Many flavoenzymes employ the TIM barrel motif to bind flavin (40). Glycolate oxidase (54), flavocytochrome b_2 (55), trimethylamine dehydrogenase (56), and old yellow enzyme (57) are all $(\beta/\alpha)_8$ barrels that tightly bind flavin mononucleotide as a coenzyme. In these enzymes the phosphate moiety of FMN binds between the β7-α7 loop and the NH_2 terminus of an additional small helix in the β8-α8 loop. Similar interactions are also observed in other TIM barrels that secure phosphate components in their substrates (58). Bacterial luciferase does not contain a small helix in the β8-α8 loop. Its absence could explain why luciferase utilizes $FMNH_2$ as a substrate and not as a prosthetic group as in other $(\beta/\alpha)_8$ flavoenzymes.

[3] T. O. Baldwin *et al.*, unpublished results.

The structure of luciferase reveals a large deep pocket entering the C-terminal end of the α subunit's β-barrel (Fig. 12). Projecting off this large central pocket is a smaller accessible cavity formed by the non-prolyl *cis* peptide bond highlighted above (Fig. 8). These pockets are sufficiently large enough to accommodate $FMNH_2$, O_2, and a long-chain aldehyde. Furthermore, the pocket is expected to exclude access water from the C4a hydroperoxyflavin intermediate and the excited flavin that is formed following the decay of the tetrahedral intermediate (8). The disordered loop is likely to achieve this task by blocking the entrance to the pocket after substrate binding, thus protecting itself from proteolysis (11, 14, 15). The current 1.5-Å resolution structure contains a few ordered water molecules in the pocket. Even though the structure of luciferase was determine in the absence of substrates, we feel confident that the active site resides within this large internal cavity of the α subunit. It should be noted that every amino acid implicated as an active center residue, either by mutagenesis or chemical modification, contacts this internal cavity. Unfortunately, attempts to soak in both oxidized and reduced flavin with and without additional substrates into the crystal have proven unsuccessful.

Folding and Assembly of Luciferase—Protein unfolding, refolding, and assembly of bacterial luciferase has been extensively studied (59–62). It has been demonstrated that separate α and β subunits, purified from recombinant *E. coli* independently bearing the *luxA* or *luxB* genes, carry out a bioluminescent reaction, but at a quantum efficiency 6 orders of magnitude below that of the heterodimer (63). Moreover, the active dimer fails to assemble when the purified folded α and β subunits are combined (64, 65). It has recently been demonstrated that purified luciferase β subunit forms a very stable β_2 homodimer that is trapped in a heterodimerization-incompetent complex and is unable to form functional heterodimers due to kinetic partitioning of the folding pathway (62). Functional dimers can assemble upon renaturation of the unfolded individual subunits (60, 62). Equilibrium unfolding studies of the luciferase heterodimer have shown that the enzyme unfolds through a well-populated non-native intermediate (59, 61). Conversion from the non-native heterodimeric intermediate to a functional enzyme is independent of protein concentration.

Some of the protein folding and assembly observations might be explained in part by the presence of the protein's two prolyl and one non-prolyl *cis* peptide bonds. It has been substantiated that *cis/trans* isomerization of the peptide bond preceding proline residues can limit the rate at which a protein can fold into its native conformation (66–68). The *cis*-Pro^{160}, which is found in both luciferase subunits, is located at the end of the hairpin loop structure that forms extensive intersubunit contacts. The *trans* isomer of this peptide bond would cause minor perturbations in the loop that would affect dimerization contacts. In both subunits the residue preceding the *cis*-proline is an aspar-

agine that contributes to dimerization by forming intersubunit hydrogen bonds (Table II).

Non-prolyl *cis* peptide bonds are scarce in nature but can be generated by mutating *cis*-proline residues in proteins (69, 70). Energy calculations predict that non-prolyl *cis* peptide bonds should destabilize a folded protein by 10–20 kJ/mol (37). Protein thermal stability measurements yield results that compare with the calculated values (70, 71). The presence of a non-prolyl *cis* peptide bond in the α subunit alone could explain why the heterodimer is apparently less stable than the β_2 homodimer (59–62).

Acknowledgments—We thank Drs. M. M. Benning and L. C. Pedersen for helping in data acquisition. We are grateful to Vicki Green for supplying the enzyme used in this study.

REFERENCES

1. Harvey, E. N. (1952) *Bioluminescence*, Academic Press, Inc., New York
2. Campbell, A. K. (1989) *Essays Biochem.* **24,** 41–76
3. Boyle, R. (1668) *Philos. Trans. R. Soc. Lond. Biol. Sci.* **2,** 581–600
4. Baldwin, T. O., Ziegler, M. M., and Powers, D. A. (1979) *Proc. Natl. Acad. Sci. U. S. A.* **76,** 4887–4889
5. Cline, T. W., and Hastings, J. W. (1972) *Biochemistry* **11,** 3359–3370
6. Meighen, E. A., and Hastings, J. W. (1971) *J. Biol. Chem.* **246,** 7666–7674
7. Becvar, J. E., and Hastings, J. W. (1975) *Proc. Natl. Acad. Sci. U. S. A.* **72,** 3374–3376
8. Baldwin, T. O., and Ziegler, M. M. (1992) in *Chemistry and Biochemistry of Flavoenzymes* (Müller, F., ed) Vol. 3, pp. 467–530, CRC Press, Inc., Boca Raton, FL
9. Cohn, D. H., Mileham, A. J., Simon, M. I., Nealson, K. H., Rausch, S. K., Bonam, D., and Baldwin, T. O. (1985) *J. Biol. Chem.* **260,** 6139–6146
10. Johnston, T. C., Thompson, R. B., and Baldwin, T. O. (1986) *J. Biol. Chem.* **261,** 4805–4811
11. Holzman, T. F., and Baldwin, T. O. (1980) *Proc. Natl. Acad. Sci. U. S. A.* **77,** 6363–6367
12. Ziegler, M. M., Rausch, S. K., Merritt, M. V., and Baldwin, T. O. (1987) in *Analytical Applications of Bioluminescence and Chemiluminescence* (Schölmerich, J., Andreesen, R., Kapp, A., Ernst, M., and Woods, W. G., eds) pp. 377–380, John Wiley & Sons, Inc., New York
13. Baldwin, T. O., Hastings, J. W., and Hastings, P. L. (1978) *J. Biol. Chem.* **253,** 5551–5554
14. Holzman, T. F., and Baldwin, T. O. (1980) *Biochem. Biophys. Res. Commun.* **94,** 1199–1206
15. Baldwin, T. O., and Riley, P. L. (1980) in *Flavins and Flavoproteins* (Yagi, K., and Yamano, T., eds) pp. 139–147, Japan Scientific Societies Press, Tokyo
16. Fisher, A. J., Raushel, F. M., Baldwin, T. O., and Rayment, I. (1995) *Biochemistry* **34,** 6581–6586
17. Conti, E., Franks, N. P., and Brick, P. (1996) *Structure* **4,** 287–298
18. Baldwin, T. O., Chen, L. H., Chlumsky, L. J., Devine, J. H., and Ziegler, M. M. (1989) *J. Biolumin. Chemilumin.* **4,** 40–48
19. Swanson, R., Weaver, L. H., Remington, S. J., Matthews, B. W., and Baldwin, T. O. (1985) *J. Biol. Chem.* **260,** 1287–1289
20. Teng, T. Y. (1990) *J. Appl. Crystallogr.* **23,** 387–391
21. Otwinowski, Z. (1993) in *Proceedings of the CCP4 Study Weekend: Data Collection and Processing* (Sawyer, L., Isaacs, N., and Bailey, S., eds) pp. 56–62, SERC Daresbury Laboratory, Daresbury, England
22. Minor, W. (1993) Purdue University, West Lafayette, IN
23. Rossmann, M. G. (ed) (1972) *The Molecular Replacement Method. A Collection of Papers on the Use of Non-Crystallographic Symmetry*, Gordon and Breach Science Publishers, New York
24. Navaza, J. (1993) *Acta Crystallogr. Sect. B* **49,** 588–591
25. Tronrud, D. E., Ten-Eyck, L. F., and Matthews, B. W. (1987) *Acta Crystallogr. Sect. B* **43,** 489–501
26. Read, R. J. (1986) *Acta Crystallogr. Sect. B* **45,** 140–149
27. Jones, T. A., Zou, J. Y., Cowan, S. W., and Kjeldgaard, M. (1991) *Acta Crystallogr. Sect. B* **47,** 110–119
28. CCP4 (1994) *Acta Crystallogr. Sect. B* **50,** 760–763
29. Ramakrishnan, C., and Ramachandran, G. N. (1965) *Biophys. J.* **5,** 909–933
30. Laskowski, R. A., MacArthur, M. W., Moss, D. S., and Thornton, J. M. (1993) *J. Appl. Crystallogr.* **26,** 283–291
31. Luzzati, V. (1952) *Acta Crystallogr. Sect. B* **5,** 802–810
32. Banner, D. W., Bloomer, A. C., Petsko, G. A., Phillips, D. C., Pogson, C. I., and Wilson, I. A. (1975) *Nature* **255,** 609–614
33. Lee, B., and Richards, F. M. (1971) *J. Mol. Biol.* **55,** 379–400
34. Janin, J., Miller, S., and Chothia, C. (1988) *J. Mol. Biol.* **204,** 155–164
35. Xin, X., Xi, L., and Tu, S. C. (1991) *Biochemistry* **30,** 11255–11262
36. Meighen, E. A. (1991) *Microbiol. Rev.* **55,** 123–142
37. Ramachandran, G. N., and Mitra, A. K. (1976) *J. Mol. Biol.* **107,** 85–92
38. Stewart, D. E., Sarkar, A., and Wampler, J. E. (1990) *J. Mol. Biol.* **214,** 253–260
39. Herzberg, O., and Moult, J. (1991) *Proteins Struct. Funct. Genet.* **11,** 223–229
40. Farber, G. K., and Petsko, G. A. (1990) *Trends Biochem. Sci.* **15,** 228–234
41. Nicoli, M. Z., Meighen, E. A., and Hastings, J. W. (1974) *J. Biol. Chem.* **249,** 2385–2392
42. Nicoli, M. Z., and Hastings, J. W. (1974) *J. Biol. Chem.* **249,** 2393–2396
43. Ziegler, M. M., and Baldwin, T. O. (1981) in *Bioluminescence and Chemiluminescence: Basic Chemistry and Analytical Applications* (Deluca, M. A., and McElroy, W. D., eds) pp. 155–160, Academic Press, New York
44. Nicoli, M. Z., Baldwin, T. O., Becvar, J. E., and Hastings, J. W. (1976) in *Flavins and Flavoproteins* (Singer, T. P., ed), pp. 87–93, Elsevier Science Publishers B.V., Amsterdam
45. Kasai, S., Matsui, K., and Nakamura, T. (1982) in *Flavins and Flavoproteins* (Massey, M., and Williams, C. H., eds) pp. 459–462, Elsevier, North-Holland, Amsterdam
46. O'Kane, D. J., Vervoort, J., Müller, F., and Lee, J. (1987) in *Flavins and Flavoproteins* (Edmondson, D. E., and McCormick, D. B., eds) pp. 641–645, Walter de Gruyter & Co., Berlin
47. Illarionov, B. A., Protopopova, M. V., Karginov, V. A., Mertvetsov, N. P., and Gitelson, J. I. (1988) *Nucleic Acids Res.* **16,** 9855
48. Baldwin, T. O., Devine, J. H., Heckel, R. C., Lin, J.-W., and Shadel, G. S. (1989) *J. Biolumin. Chemilumin.* **4,** 326
49. Moore, S. A., James, M. N. G., O'Kane, D. J., and Lee, J. (1993) *EMBO J.* **12,** 1767–1774
50. Moore, S. A., and James, M. N. G. (1995) *J. Mol. Biol.* **249,** 195–214
51. Moore, S. A., and James, M. N. G. (1994) *Protein Sci.* **3,** 1914–1926
52. Zhang, X., Wozniak, J. A., and Matthews, B. W. (1995) *J. Mol. Biol.* **250,** 527–552
53. Kishan, K. V. R., Zeelen, J. P., Noble, M. E. M., Borchert, T. V., and Wierenga, R. K. (1994) *Protein Sci.* **3,** 779–787
54. Lindqvist, Y. (1989) *J. Mol. Biol.* **209,** 151–166
55. Xia, Z.-X., and Mathews, F. S. (1990) *J. Mol. Biol.* **212,** 837–863
56. Lim, L. W., Shamala, N., Mathews, F. S., Steenkamp, D. J., Hamlin, R., and Xuong, N. h. (1986) *J. Biol. Chem.* **261,** 15140–15146
57. Fox, K. M., and Karplus, P. A. (1994) *Structure* **2,** 1089–1105
58. Wilmanns, M., Hyde, C. C., Davies, D. R., Kirschner, K., and Jansonius, J. N. (1991) *Biochemistry* **30,** 9161–9169
59. Ziegler, M. M., Goldberg, M. E., Chaffotte, A. F., and Baldwin, T. O. (1993) *J. Biol. Chem.* **268,** 10760–10765
60. Baldwin, T. O., Ziegler, M. M., Chaffotte, A. F., and Goldberg, M. E. (1993) *J. Biol. Chem.* **268,** 10766–10772
61. Clark, A. C., Sinclair, J. F., and Baldwin, T. O. (1993) *J. Biol. Chem.* **268,** 10773–10779
62. Sinclair, J. F., Ziegler, M. M., and Baldwin, T. O. (1994) *Nature Struct. Biol.* **1,** 320–326
63. Waddle, J., and Baldwin, T. O. (1991) *Biochem. Biophys. Res. Commun.* **178,** 1188–1193
64. Waddle, J. J., Johnston, T. C., and Baldwin, T. O. (1987) *Biochemistry* **26,** 4917–4921
65. Sinclair, J. F., Waddle, J. J., Waddill, E. F., and Baldwin, T. O. (1993) *Biochemistry* **32,** 5036–5044
66. Brandts, J. F., Halvorson, H. R., and Brennan, M. (1975) *Biochemistry* **14,** 4953–4963
67. Koide, S., Dyson, H. J., and Wright, P. E. (1993) *Biochemistry* **32,** 12299–12310
68. Hodel, A., Rice, L. M., Simonson, T., Fox, R. O., and Brünger, A. T. (1995) *Protein Sci.* **4,** 636–654
69. Mayr, L. M., Willbold, D., Rösch, P., and Schmid, F. X. (1994) *J. Mol. Biol.* **240,** 288–293
70. Schultz, D. A., and Baldwin, R. L. (1992) *Protein Sci.* **1,** 910–916
71. Mayr, L. M., Landt, O., Hahn, U., and Schmid, F. X. (1993) *J. Mol. Biol.* **231,** 897–912
72. Kraulis, P. J. (1991) *J. Appl. Crystallogr.* **24,** 946–950
73. Nicholls, A., Sharp, K. A., and Honig, B. (1991) *Proteins Struct. Funct. Genet.* **11,** 281–296
74. Smith, T. J. (1995) *J. Mol. Graphics* **13,** 122–125